NANO LETTERS
Letter
Cite This: Nano Lett. 2018, 18, 449−454
pubs.acs.org/NanoLett

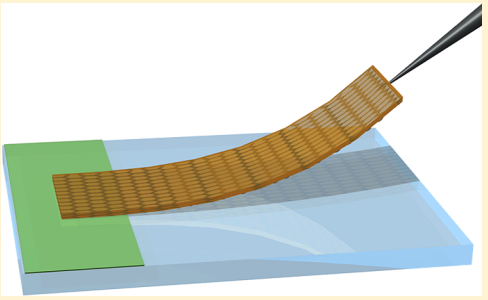
Measuring and Manipulating the Adhesion of Graphene

Marc Z. Miskin,[†,‡] Chao Sun,[§,∥] Itai Cohen,[†,‡] William R. Dichtel,[*,§,∥] and Paul L. McEuen[*,†,‡]

[†]Laboratory of Atomic and Solid State Physics, Cornell University, Ithaca, New York 14853, United States
[‡]Kavli Institute at Cornell for Nanoscale Science, Cornell University, Ithaca, New York 14853, United States
[§]Department of Chemistry, Northwestern University, 2045 Sheridan Road, Evanston, Illinois 60208, United States
[∥]Department of Chemistry and Chemical Biology, Cornell University, Ithaca, New York 14853, United States

Supporting Information

ABSTRACT: We present a technique to precisely measure the surface energies between two-dimensional materials and substrates that is simple to implement and allows exploration of spatial and chemical control of adhesion at the nanoscale. As an example, we characterize the delamination of single-layer graphene from monolayers of pyrene tethered to glass in water and maximize the work of separation between these surfaces by varying the density of pyrene groups in the monolayer. Control of this energy scale enables high-fidelity graphene-transfer protocols that can resist failure under sonication. Additionally, we find that the work required for graphene peeling and readhesion exhibits a dramatic rate-independent hysteresis, differing by a factor of 100. This work establishes a rational means to control the adhesion of 2D materials and enables a systematic approach to engineer stimuli-responsive adhesives and mechanical technologies at the nanoscale.



KEYWORDS: *Adhesion, 2D materials, graphene, delamination*

Downloaded via CORNELL UNIV on October 23, 2019 at 18:02:41 (UTC).
See https://pubs.acs.org/sharingguidelines for options on how to legitimately share published articles.

Atomic membranes such as graphene and MoS_2 provide unparalleled combinations of electronic, optical, chemical, and mechanical properties in single-atom or few-atom thick forms.[1] Their use in scientific and technological applications depends critically on controlling their adhesion to each other and/or other substrates since adhesive forces control processes such as wrinkling,[2] delamination,[3] exfoliation,[4] folding,[5] layering,[1] and tribological behavior.[6,7] For example, overcoming interlayer adhesion by mechanical exfoliation was essential for the initial isolation of single graphene sheets. More generally, controlling adhesive phenomena is central to the development of two-dimensional materials as biosensors,[8] electrodes,[9] and devices based on kirigami and origami techniques.[5,10] Yet despite its critical importance, methods to characterize and control adhesion in two-dimensional systems are lacking.[11,12]

Here we present a systematic approach to measure the surface energies between two-dimensional materials and substrates that is simple, versatile, precise, and performed in application-relevant environments. To demonstrate the technique, we measure the work required to separate single-layer graphene from a variety of molecular monolayers bound to glass and show that separation energies can be tuned by two orders of magnitude. In addition to delamination, we characterize the reattachment processes and find that there is significant hysteresis between the two, showing that attaching/peeling behavior for atomic membranes is thermodynamically irreversible.

Figure 1A illustrates the fabrication sequence for the devices studied. Aluminum oxide is deposited onto the surface of a borosilicate glass coverslip, and trenches are patterned into it using lithographic techniques (see Supporting Information for details). The aluminum oxide serves as a release layer, while the exposed glass in the trenches is chemically treated to act as adhesive regions. Next, 3-aminopropyltriethoxysilane (APTES) is introduced from the vapor phase to functionalize the exposed glass with reactive amine-terminated propyl chains. Treatment of the patterned APTES with a solution of *N*-hydroxysuccinimidyl (NHS) ester-containing compounds, such as NHS pyrene butyrate (Figure 1C) or NHS acetate (see below), elaborates the organic monolayer through amide bonds. We then transfer monolayer graphene, grown by chemical vapor deposition, onto the substrates. The graphene is patterned into rectangles by using a 2 μm-thick layer of SU-8 photoresist. One end of the cantilever is adhered to the organic monolayer, as shown in the figure. Note the SU-8 layer is left on top of the graphene. It serves as a cantilever of known stiffness that is used to measure the work done by surface forces, as discussed below. Finally, dilute aqueous acid is used to etch the aluminum oxide and release the graphene from the surface, except where anchored by the organic adhesive layer.[10]

Figure 1B shows a reflection optical micrograph of five graphene/SU-8 cantilevers of varying widths in water. The

Received: October 12, 2017
Revised: December 6, 2017
Published: December 22, 2017

© 2017 American Chemical Society

DOI: 10.1021/acs.nanolett.7b04370
Nano Lett. 2018, 18, 449−454

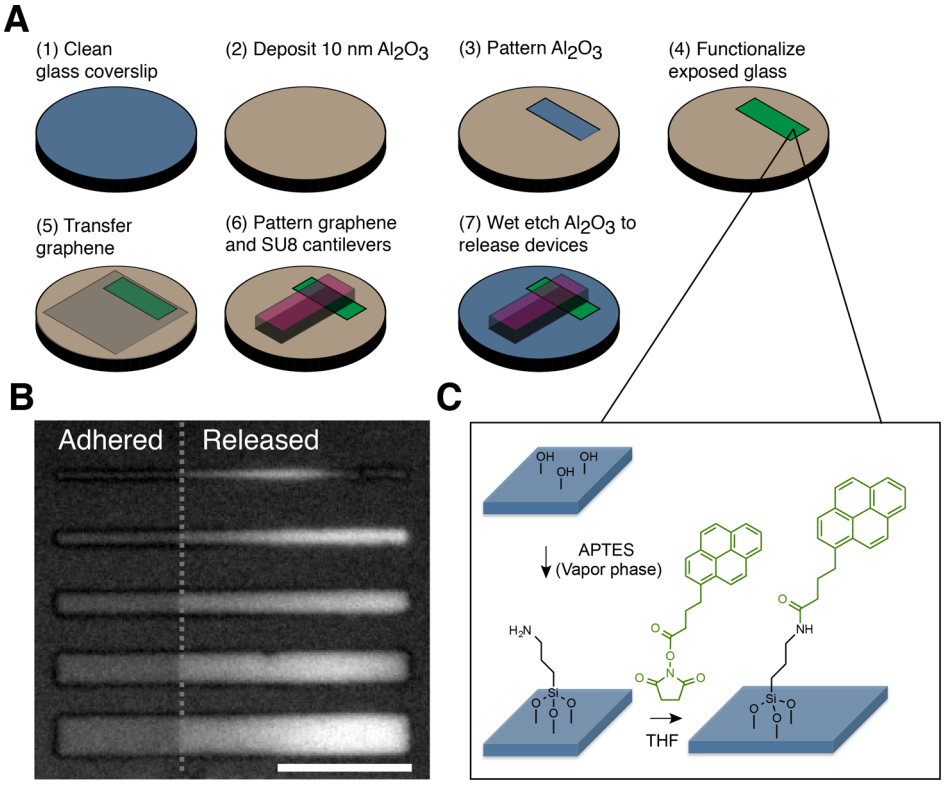


Figure 1. Patterning an area for graphene adhesion with a pyrene-containing monolayer. (A) Process flow for patterning regions of a glass substrate with a molecular monolayer to mediate graphene adhesion. (B) Reflection-mode optical micrograph of five parallel graphene/SU-8 cantilevers bound by the patterned pyrene monolayer in water after the Al_2O_3 release layer was removed. The lighter regions to the right of the adhesion area are the released portions of the cantilevers. Scale bar: 25 μm. (C) Approach for forming functionalized monolayers in the adhesion trench. 3-Aminopropyltriethoxysilane (APTES) is introduced to the surface from the vapor phase. Next, *N*-hydroxysuccinimide pyrene butyrate in a tetrahydrofuran (THF) solution is introduced to the surface and reacts with the surface amine groups.

dark regions on the left of each rectangular strip are adhered to the pyrene-containing monolayer. The lighter regions to the right of the adhered area are released from the surface. Variations in brightness indicate changes in height because of light interference between the glass substrate and the graphene/SU-8 cantilever.[10] The cantilever sticks to the pyrene monolayer even under fluid flow, and these cantilevers remain attached without obvious degradation in water for weeks. They also remain attached for at least several days over a range of ionic strengths (0−1 M HCl) and in the presence of added surfactants (sodium dodecylbenzenesulfonate). In contrast, cantilevers bind much more weakly to bare glass and are easily washed away in flow or detached by weak mechanical forces.

The work of separation can be measured by using a micromanipulator to peel the cantilever off the surface, as illustrated schematically in Figure 2A (see also Supplemental Video S1). We lift the free end of the graphene/SU-8 cantilever quasi-statically causing the cantilever to first bend, then peel, and finally detach (Figure 2B). The peeling process is stable such that the interface between the adhered and released areas does not move if the probe is halted. The white bands in Figure 2B are interference fringes between the coverslip and the cantilever. Each bright fringe corresponds to an incremental height increase of $\lambda/2$ = 224 nm[10] and thus provides an optical readout of the cantilever's height $h(x)$ (Figure 2C,D). Indeed, optical interferometry is well established as a means of extracting deformation profiles during delamination experiments at the macroscale and is increasingly being used when studying the adhesion of 2D materials.[13−15] Moreover, as both the graphene and SU8 are visible via optical microscopy, we inspect devices to determine that the graphene−surface interface delaminates, rather than the graphene−SU8 interface.

By fitting $h(x)$ data to a parabola, we extract two key parameters: the position of the interface between the adhered and free regions of graphene (x_o), and the curvature in the cantilever at this interface (κ) . These are shown as a function of the probe height in Figure 2E. There are three regimes for delamination: loading, peeling onset, and a steady-state peeling. First, the interface is fixed, and the curvature in the free region increases in proportion to the applied displacement from the micromanipulator (Figure 2B, images 1−2). Next, peeling begins. The length of the adhered region decreases and the cantilever curvature continues to increase (Figure 2B, image 3). Finally, the peeling reaches a steady state at which the curvature stays constant while the peeling front moves, indicating a constant work of separation (Figure 2B, images 4−5). This regime continues until the cantilever detaches (image 6).

On the basis of energy conservation, we define an effective work required for peeling surfaces apart, γ_{peel}, from the curvature κ in the steady-state peeling regime, as well as the Young's modulus (E) and thickness (t) of the SU-8 cantilever (see the Supporting Information for a derivation):

$$\gamma_{peel} = \frac{E_y t^3 k}{24} \quad (1)$$

DOI: 10.1021/acs.nanolett.7b04370
Nano Lett. 2018, 18, 449−454

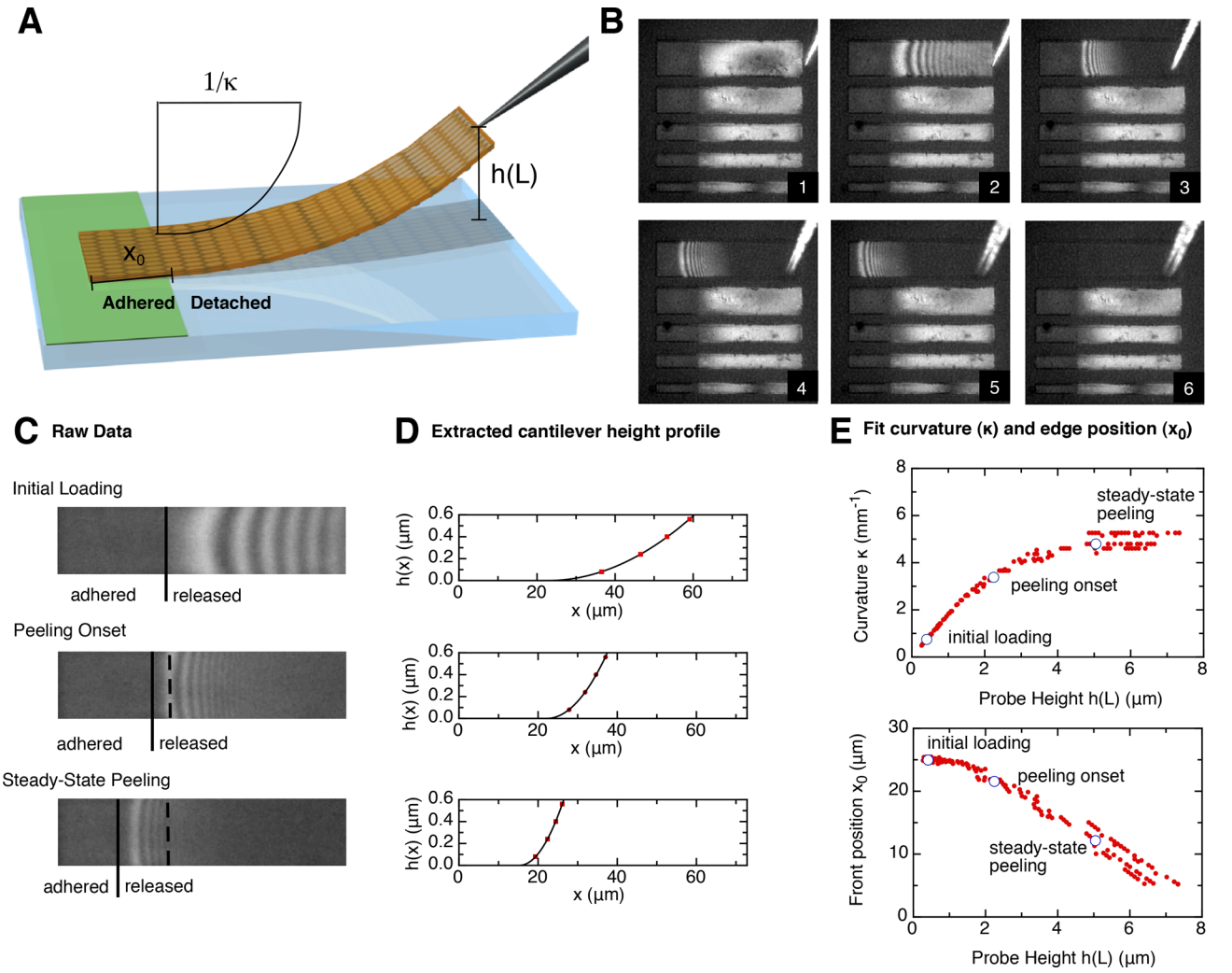


Figure 2. Applied force delaminates the cantilever from the adhered region. (A) Schematic of applying upward force to a partially adhered graphene/SU-8 cantilever using a micromanipulator. The edge position x_o is defined as the interface between the bound and the free portions of graphene with respect to the left end of the cantilever. The height $h(L)$ is the height of the manipulator, and κ is the curvature of the cantilever. (B) Series of reflection white-light micrographs that shows the delamination process (see also Supplemental Video S1) These images and the video have undergone linear contrast adjustment. (C) Reflection white-light micrographs of a graphene/SU-8 cantilever at three stages of peeling: during the initial loading (top), the onset of the cantilever peeling (center), and steady-state peeling (bottom). The solid line marks the delamination front position (x_0), while the dashed lines delineate the region of the substrate that was functionalized. (D) Cantilever height $h(x)$ extracted from the interference pattern, along with a parabolic fit. Points represent the location for each interface peak averaged over the width of the cantilever; error bars on the peak location are the size of the symbol. (E) Edge position x_o (bottom) and the cantilever's curvature κ (top) as a function of the probe height $h(L)$ as peeling progresses.

We note that this energy per unit area encompasses the full response from any microscopic forces that resist separation of the two layers: in addition to the thermodynamically reversible surface energies, it can include dissipative effects, effects from local spatial inhomogeneity, or long-range surface−surface interaction forces. In short, it defines the practical work required to separate two surfaces from one another, given a set of environmental conditions. For the data shown in Figure 2, this analysis, given a thickness of 2 μm and an established literature value of 3.5 GPa for the Young's modulus of SU8 photoresist,[16] provides γ_{peel} = 0.1 N/m, which is consistent with previous estimates and measurements of van der Waals mediated bonding between interfaces.[10]

We observe that the measured work required to separate graphene from the substrate varies with the chemical composition of the binding monolayer. Figure 3 shows measurements of γ_{peel} for a variety of surfaces ranging from bare glass (minimal work of separation) to a specific mixed monolayer of pyrene butyrate and acetate groups (maximum work of separation). Acetate modulates the pyrene density of the monolayer without drastically changing surface hydrophobicity (Figure S3). The work required to separate the surfaces is maximized when a 40 mol % pyrene butyrate/60 mol % acetate activated ester solution is used to form the molecular monolayer. Notably, less work is required to separate monolayers containing either 100% acetate or 100% pyrene from graphene. As a control, we also tested SU8 cantilevers, without graphene, bonded to glass. We found that these could not be detached, and instead bent until failure, indicating that it is the graphene that sets the scale of the measured surface energy.

The nontrivial variations of the work of separation indicate that a variety of mechanisms are at play. For instance, the data indicate that pyrene butyrate groups cannot fully engage the

DOI: 10.1021/acs.nanolett.7b04370
Nano Lett. 2018, 18, 449−454

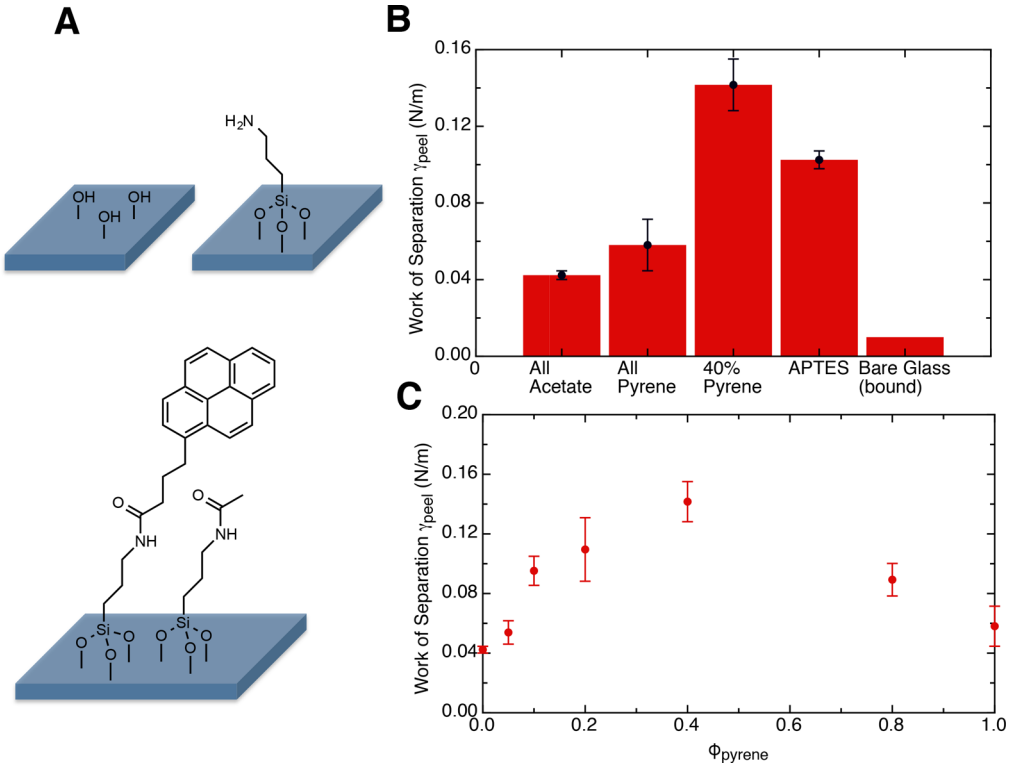


Figure 3. Optimizing adhesion using molecular adhesives. (A) Examples of surface chemistries tested for their strength of adhesion to graphene. Surface-bound pyrenes are designed as graphene-binding groups, and acetates are used to limit the pyrene concentration in the monolayer. Amine-terminated monolayers and unfunctionalized glass were also evaluated. (B) Average values for the work of separation and the error on the mean for the different surface treatments. The value measured for unmodified glass represents an upper bound set by the resolution limit of our measurement for the cantilever stiffness used. (C) Work of separation for surfaces treated with different ratios of pyrene and acetate in the monolayers. Φ_{pyrene} corresponds to the mol % of pyrene in the solution used to functionalize the APTES monolayer, with NHS-acetate making up the remainder. Error bars indicate the error on the mean over seven devices in two fabrication batches.

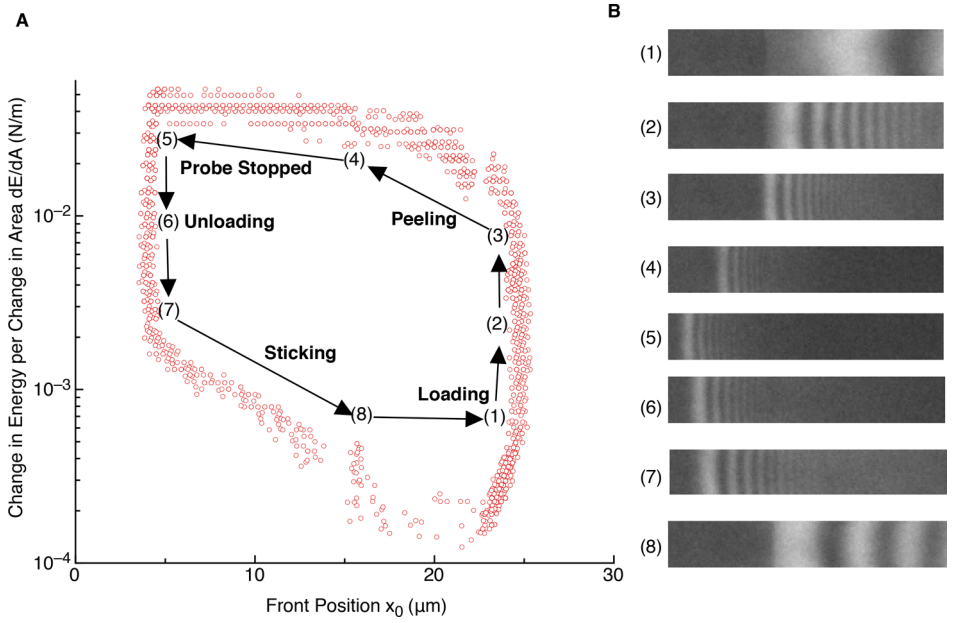


Figure 4. Irreversibility and hysteresis of adhesion. (A) Energetics of a complete delamination/readhesion cycle plotted as the elastic energy changes per change in area (dE/dA) relative to the position of the peeling front x_0. (B) Reflection white-light micrographs corresponding to the numbered stages of the cycle (1–8). See also Supplemental Video S2.

graphene surface when incorporated at too high a density[17−19] even though pyrene−graphene interactions are enthalpically favored over pyrene−pyrene interactions by 155 kJ/mol.[20,21] Unmodified APTES monolayers also bind to graphene relatively strongly, perhaps through cation−π interactions of protonated amines in the monolayer.[22] In contrast, graphene

DOI: 10.1021/acs.nanolett.7b04370
Nano Lett. 2018, 18, 449−454

sticks very weakly to unmodified glass, with at least an order of magnitude less work required for separation than the strongest adhesives (Figure 3B).

The adhesion properties for the graphene−surface bond at a given cantilever are robust and reproducible. Fatigue is not observed when repeatedly peeling and resticking the same cantilever, indicating high-fidelity adhesion and negligible damage to the molecular monolayer. Graphene adhered to the 40 mol % pyrene monolayer remains adhered and appears undamaged after bath sonication in water or organic solvents typically used for substrate cleaning (Figure S6). This procedure heavily damages or completely delaminates graphene transferred to most substrates, a major inconvenience for device fabrication.[23] Taken together, the results shown in Figures 1−3 provide a straightforward approach to characterizing the strength, resilience, and durability of bonds between atomic membranes and different substrate surface chemistries in application environments.

Finally, we explore the reproducibility and hysteresis of the peeling process (see Supplemental Video S2). Because delamination is quasi-static, we can stop peeling at any time, reverse the loading direction, and observe that the graphene readheres to the functionalized surface. In Figure 4A, the change in elastic energy stored in the cantilever per change in area is plotted (on a log scale) against the location of the peeling front x_o over a complete delamination and reattachment cycle. After peeling reaches steady state, we stop and unload the cantilever. Initially, the cantilever curvature decreases, but the interface between the adhered and released regions stays fixed. When the curvature of the cantilever is approximately ten times smaller than that observed during steady-state peeling, the interface moves backward (x_0 increases) and the graphene readheres to the molecular monolayer. Thus, we find peeling is highly hysteretic with roughly 100 times more energy required to delaminate the cantilever than is recovered when readhered. We note similar hysteresis has been observed in the delamination of MoS_2 sheets from silicon substrates.[24] This loading and unloading behavior is highly reproducible and can be repeated hundreds of times with no detectable changes in the peeling or sticking behavior. However, if the cantilever is completely detached from the surface, it will not readily readhere. Finally, we find no significant differences in the delamination or readhesion behavior associated with rate when the peeling rate is varied over three orders of magnitude.

Hysteretic behavior in adhesion processes is ubiquitous and has been observed in systems ranging from multivalent interactions between molecules[25−27] to Gecko feet.[28,29] Figure 4 shows that hysteresis is present in the bonding of atomic membranes to substrates as well. Moreover, the work done by surface forces depends on the front position, for instance, in advancing from position 3 to 4, presenting another interesting and unexplained characteristic of the graphene−surface interaction. In general, the mechanisms behind such hysteresis are often poorly understood, and identifying the cause in this system is a challenge for future experiments and theories.

This study establishes how to measure and control the adhesion mechanics of 2D materials through a platform that is well suited to many other nanofabrication techniques and device measurements. Although here we focused on pyrene−graphene interactions in water, the approach is general and requires only a substrate compatible with lithographic patterning methods. In principle, all of these experiments could be reproduced in air or vacuum by using a suitable release layer. Broadly, our approach makes it possible to probe the influence of surfactants, solution properties, and other surface chemistries. Research into the molecular mechanisms of atomic membrane adhesion will enable the control of bonding, layering, and exfoliation of 2D materials. For example, the ability to dial in specific failure strengths opens the door to controlled and reproducible transfer protocols. The discovery of a dramatic difference between the work associated with peeling and readhesion presents new opportunities to explore the fundamental science of adhesion in two-dimensional materials. We further envision opportunities for switching adhesion properties by engineering adhesive molecules that change in response to optical, chemical, or thermal signals. In each of these cases, our experimental protocol can provide the necessary information to design and tune interfacial adhesives for atomically thin materials.

■ ASSOCIATED CONTENT

Supporting Information

The Supporting Information is available free of charge on the ACS Publications website at DOI: 10.1021/acs.nanolett.7b04370.

Using a micromanipulator to peel the cantilever off the surface (AVI)

Reproducibility and hysteresis of the peeling process (AVI)

Experimental procedures (PDF)

■ AUTHOR INFORMATION

Corresponding Authors

*E-mail: wdichtel@northwestern.edu.

*E-mail: plm23@cornell.edu.

ORCID

Marc Z. Miskin: 0000-0002-0905-8706

William R. Dichtel: 0000-0002-3635-6119

Author Contributions

M.M. and C.S. contributed equally to the research. W.D. and P.M. conceived of the study. C.S. developed the surface functionalization. C.S. and M.M. carried out the device fabrication. M.M. and C.S. conducted the measurements. M.M. analyzed the data. All authors contributed to writing the manuscript.

Notes

The authors declare no competing financial interest.

■ ACKNOWLEDGMENTS

We thank P. Rose, K. Dorsey, and H. Gao for fabrication assistance and graphene growth. This work was supported by the Cornell Center for Materials Research (National Science Foundation, NSF, grant DMR-1719875) and the Kavli Institute at Cornell for Nanoscale Science. This work was performed in part at the Cornell NanoScale Facility, a member of the National Nanotechnology Coordinated Infrastructure (NNCI), which is supported by the National Science Foundation (Grant ECCS-1542081).

■ REFERENCES

(1) Novoselov, K. S.; Mishchenko, A.; Carvalho, A.; Castro Neto, A. H. *Science* **2016**, *353*, 9439.

DOI: 10.1021/acs.nanolett.7b04370
Nano Lett. 2018, 18, 449−454

(2) Pereira, V. M.; Castro Neto, A. H.; Liang, H. Y.; Mahadevan, L. *Phys. Rev. Lett.* **2010**, *105*, 156603.
(3) Koenig, S. P.; Boddeti, N. G.; Dunn, M. L.; Bunch, J. S. *Nat. Nanotechnol.* **2011**, *6*, 543−546.
(4) Park, S.; Ruoff, R. S. *Nat. Nanotechnol.* **2009**, *4*, 217−224.
(5) Shenoy, V. B.; Gracias, D. H. *MRS Bull.* **2012**, *37*, 847−854.
(6) Lee, C.; Li, Q.; Kalb, W.; Liu, X. Z.; Berger, H.; Carpick, R. W.; Hone, J. *Science* **2010**, *328*, 76−80.
(7) Kawai, S.; Benassi, A.; Gnecco, E.; Sode, H.; Pawlak, R.; Feng, X.; Mullen, K.; Passerone, D.; Pignedoli, C. A.; Ruffieux, P.; Fasel, R.; Meyer, E. *Science* **2016**, *351*, 957−961.
(8) Kuila, T.; Bose, S.; Khanra, P.; Mishra, A. K.; Kim, N. H.; Lee, J. H. *Biosens. Bioelectron.* **2011**, *26*, 4637−4648.
(9) Kim, K. S.; Zhao, Y.; Jang, H.; Lee, S. Y.; Kim, J. M.; Kim, K. S.; Ahn, J.-H.; Kim, P.; Choi, J.-Y.; Hong, B. H. *Nature* **2009**, *457*, 706−710.
(10) Blees, M. K.; Barnard, A. W.; Rose, P. A.; Roberts, S. P.; McGill, K. L.; Huang, P. Y.; Ruyack, A. R.; Kevek, J. W.; Kobrin, B.; Muller, D. A.; McEuen, P. L. *Nature* **2015**, *524*, 204−207.
(11) Bunch, J. S.; Dunn, M. L. *Solid State Commun.* **2012**, *152*, 1359−1364.
(12) Van Engers, C. D.; Cousens, N. E. A.; Babenko, V.; Britton, J.; Zappone, B.; Grobert, N.; Perkin, S. *Nano Lett.* **2017**, *17*, 3815−3821.
(13) Na, S. R.; Suk, J. W.; Tao, L.; Akinwande, D.; Ruoff, R. S.; Huang, R.; Liechti, K. M. *ACS Nano* **2015**, *9*, 1325−1335.
(14) Cao, Z.; Tao, L.; Akinwande, D.; Huang, R.; Liechti, K. M. *Int. J. Solids Struct.* **2016**, *84*, 147−159.
(15) Na, S. R.; Suk, J. W.; Ruoff, R. S.; Huang, R.; Liechti, K. M. *ACS Nano* **2014**, *8*, 11234−11242.
(16) Robin, C. J.; Vishnoi, A.; Jonnalagadda, K. N. *J. Microelectromech. Syst.* **2014**, *23*, 168−180.
(17) Lochmuller, C. H.; Colborn, A. S.; Hunnicutt, M. L.; Harris, J. M. *J. Am. Chem. Soc.* **1984**, *106*, 4077−4082.
(18) Douglas, J. F.; Dudowicz, J.; Freed, K. F. *Phys. Rev. Lett.* **2009**, *103*, 135701.
(19) Ulman, A. *Chem. Rev.* **1996**, *96*, 1533−1554.
(20) Takeuchi, H. *Comput. Theor. Chem.* **2013**, *1021*, 84−90.
(21) Grimme, S. *J. Comput. Chem.* **2004**, *25*, 1463−1473.
(22) Gebbie, M. A.; Wei, W.; Schrader, A. M.; Cristiani, T. R.; Dobbs, H. A.; Idso, M.; Chmelka, B. F.; Waite, J. H.; Israelachvili, J. N. *Nat. Chem.* **2017**, *9*, 473−479.
(23) Ciesielski, A.; Samori, P. *Chem. Soc. Rev.* **2014**, *43*, 381−398.
(24) Lloyd, D.; Liu, X.; Boddeti, N.; Cantley, L.; Long, R.; Dunn, M. L.; Bunch, J. S. *Nano Lett.* **2017**, *17*, 5329−5334.
(25) Jennissen, H. P.; Botzet, G. *Int. J. Biol. Macromol.* **1979**, *1*, 171−179.
(26) Huskens, J. *Curr. Opin. Chem. Biol.* **2006**, *10*, 537−543.
(27) Mann, J. A.; Dichtel, W. R. *ACS Nano* **2013**, *7*, 7193−7199.
(28) Bhushan, B. *Langmuir* **2012**, *28*, 1698−1714.
(29) Chaudhury, M. K.; Owen, M. J. *Langmuir* **1993**, *9*, 29−31.

DOI: 10.1021/acs.nanolett.7b04370
Nano Lett. 2018, 18, 449−454